Available online at www.sciencedirect.com
SCIENCE DIRECT
Surface Science 600 (2006) 2505–2509
SURFACE SCIENCE
www.elsevier.com/locate/susc

Structure of the hydrogen stabilized MgO(1 1 1)-(1 × 1) surface from low energy electron diffraction (LEED)

H.C. Poon, X.F. Hu, S.E. Chamberlin, D.K. Saldin, C.J. Hirschmugl *

Department of Physics and Laboratory for Surface Studies, University of Wisconsin Milwaukee, Milwaukee, WI 53211, USA

Received 10 February 2006; accepted for publication 6 April 2006
Available online 11 May 2006

Abstract

A structural study has been performed on the MgO(1 1 1)-(1 × 1) surface by low energy electron diffraction (LEED) using experimental data obtained with a delay-line-detector LEED (DLD-LEED) system to minimize electron damage. It was found that the surface is terminated by a hydroxide layer with the top O–Mg interlayer spacing equal to 1.02 Å, which is close to the spacings between Mg and O planes in bulk brucite crystals ($Mg(OH)_2$). This is in good agreement with a recent study using photoelectron diffraction (PhD) spectroscopy and density functional theory calculation (DFT) [V.K. Lazarov, R. Plass, H.-C. Poon, D.K. Saldin, M. Weinert, S.A. Chambers, M. Gajdardziska-Josifovska, Phys. Rev. B 71 (2005) 115434]. The second interlayer spacing shows a small expansion of 3% and the third is bulk-like, while the DFT calculation predicted that the spacings below the top one are all bulk-like. This result clearly favors hydroxylation [K. Refson, R.A. Wogelius, D.G. Fraser, M.C. Payne, M.H. Lee, V. Milman, Phys. Rev. B 52 (1995) 10823] as a way of stabilizing the MgO(1 1 1) surface at low temperature over metallization, which has a top layer spacing of 0.86 Å for O termination and 1.25 Å for Mg termination [Lazarov et al. 2005; T. Tsukada, T. Hoshino, Phys. Soc. Jpn. 51 (1982) 2562, J. Goniakowski, C. Noguera, Phys. Rev. B 60 (1999) 16120].

Keywords: Electron solid interactions; Scattering; Diffraction; Low energy electron diffraction; Magnesium oxides

1. Introduction

Recent works on the MgO(1 1 1) polar surface show that a number of air-stable reconstructions exist above 1200 °C [5]. For samples annealed to temperatures below 950 °C, the surface is unreconstructed [1]. However, the surface energy of the bulk terminated (1 × 1) surface would be divergent without some kind of stabilization. There have been first-principle calculations which suggest that the MgO(1 1 1)-(1 × 1) polar surface is either stabilized by metallization [3,4] or hydroxylation [2]. A more recent study by density functional theory (DFT) considered the different models with various amounts of H above or beneath the outermost MgO layer, and also without H. This study [1] shows that, amongst these possible models, the hydroxide-terminated surface not only has the lowest surface energy, but also gives the best fit to experimental photoelectron diffraction (PhD) data. Since the surface structure depends on the amount of H and the positions of the H atoms, the DFT analysis can consider only a finite number of models. The PhD data set is also too small to allow a proper structural search.

The purpose of the present work is to perform a structural search on MgO(1 1 1)-(1 × 1) by low energy electron diffraction (LEED). A delay-line-detector LEED (DLD-LEED) system was used to minimize the electron-induced dissociations. The data were collected over a cumulative energy range of over 900 eV, making it possible to search over the complete parameter space of the top few layers.

2. Experimental details

The MgO(1 1 1) single crystal sample was obtained from MTI Corporation. The surface was EPI-polished with the surface roughness <5 Å. The sample was annealed at 600 °C in air for 12 h to retrieve the (1 × 1) surface

* Corresponding author. Tel.: +1 414 229 5748; fax: +1 414 229 5589.
E-mail address: cjhirsch@uwm.edu (C.J. Hirschmugl).

0039-6028/$ - see front matter © 2006 Elsevier B.V. All rights reserved.
doi:10.1016/j.susc.2006.04.010

termination structure. It was then mounted in the UHV chamber for the LEED measurement.

The LEED measurements were performed with a low-current, pulse-counting and high-count-rate delay line detector LEED (DLD-LEED) system [6]. It uses a low-current electron gun, microchannel plates for charge amplification, and delay line anode planes for signal detection, reducing the electron-induced dissociations. For instance, the electron dose is only 5.6×10^7 with the beam current of 150 fA, the electron energy of 108 eV, and the exposure time of 60 s, which cannot be achieved by standard LEED systems [7]. The details of the DLD-LEED system and the comparisons with other systems can be found in Ref. [7].

It is instructive to estimate how much electron beam damage can occur assuming single scattering events for a full monolayer coverage of adsorbates. The incident electrons either (1) scatter from the adsorbates or substrate, returning diffracted intensities to the detector, or (2) ionize and possibly desorb the adsorbate, losing energy and not returning to the detector. While the latter electrons do not directly contribute to the LEED *I–V* intensities, they can change the local or long-range geometry (by modifying or desorbing adsorbates) for the subsequently diffracted electrons. Electron stimulated desorption cross sections for hydrogen are surface dependent and are reported to range between 1×10^{-18} m^2 and 1×10^{-20} m^2 for different Si faces [8,9] for energies between 100 and 500 eV. For comparison, scattering cross sections and ionizing cross sections for water are between $4-7 \times 10^{-20}$ m^2 and $2-4 \times 10^{-20}$ m^2 for electrons with energies between 100 and 300 eV [10,12,11]. Thus 50% of all electron-adsorbate interactions can result in an ionized and potentially desorbed or dissociated adsorbate. In the present experiment the sample is exposed to approximately 2×10^9 electrons for the duration of one energy scan (100–350 eV). Assuming the electron beam is between 50 and 250 μm in diameter, as is appropriate for the DLD–LEED, and an average scattering cross section of 5×10^{-20} m^2, 2–10% of the adsorbates scatter electrons, leaving 1–5% of the adsorbates ionized. This percentage of desorbed or dissociated species is acceptable. If this electron dose is increased to 5×10^{13}, electrons (as used in recent studies of water on MgO(100) [13] taking into account a nanoampere beam and appropriate acquisition time), all of the adsorbates would have scattered more than one electron and there would be severe electron damage. Ferry et al. [13] did not mention the size of the electron beam or discuss or show the reproducibility of the *I–V* curves, however, the superstructure spots were clearly observable for the entire experiment. Thus, it is likely that the electron beam had a larger diameter than the present experiment and perhaps did not dissociate a large fraction of the adsorbates. However, it is worth mentioning that in order to generate the theoretical *I–V* curves an unphysical inner potential of 18.5 eV was required to match the experimental results [13]. This suggests that the electron exposure was inducing sample charging which could have an impact on the structures of polar adsorbates.

Since all stray electrons can be detected by the DLD-LEED, all electron sources (i.e., ion gauge, ion pump) are either turned off or isolated from the UHV chamber. The residual pressure of the UHV chamber, maintained by a Varian V-250 turbo pump, was better than 1×10^{-9} torr. The sample temperature was held at 300 K. In a 7-h LEED measurement, AES did not detect any accumulation of surface contaminations (i.e., carbon) or change in peak ratios.

The output of the LEED apparatus is a set of 32-bit (color depth) 1028×1028 pixel data files representing the observed diffraction pattern at each energy. The electron energy ranges from 50 eV to 474 eV in 4 eV steps. The data processing software aims to recover from the set of these large data files a series of *I–V* curves corresponding to each Bragg beam. It does this in three stages. In the first stage, a data-acceptance software window of a given size is moved over the detector for any given energy to locate the brightest areas, assumed to be the Bragg spots. The counts within each window are fitted to a two-dimensional gaussian. The quality of a peak is indicated both by its position within the window and the fitting error (a Bragg spot is assumed well located if the peak is near the center of the window). The peak positions of two of the brighter spots of good quality at the same electron energy are chosen as the reference points to be used in the second stage – the data collection stage. In this second stage, the two reference points from the first stage are used to generate the pixel coordinates of each beam in the LEED pattern at the reference energy. The trajectory of each beam as a function of energy is given by

$$\frac{|t - t_0|}{R} = \frac{g}{k} \tag{1}$$

where k is the wave number of electron. g is the magnitude of the reciprocal space vector of the beam, R is the radius of the screen, t is the distance (measured along the trajectory) of the beam from a given axis in the LEED pattern (say the y axis), and t_0 is the corresponding distance between the center of the LEED pattern and the same axis. The geometry of the LEED setup and the LEED pattern

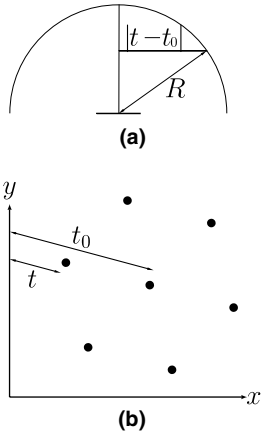

Fig. 1. Geometry of (a) the LEED setup and (b) the LEED pattern on detector.

on detector are illustrated in Fig. 1. As a function of energy, the window is moved along the trajectory of each beam and the sum of the counts inside each window are summed to give the intensity associated with that beam as a function of energy. The final stage is the correction stage, that locates the peaks of high quality close to the trajectory generated at the second stage. A straight line is fitted to these peaks. According to Eq. 1, $|t - t_0|$ is proportional to the inverse of k. The constants R and t_0 can be found from fitting the values of t and k of these peaks to a straight line. The intensities are then collected along the new trajectories and the background is subtracted off the raw intensities [14].

The energy range of the I–V curves is limited by both the size of the detector and the noise at high energy. At low energy, the high-order beams are deflected outside the detector while at high energy, the elastic intensity decreases such that the noise/signal ratio becomes very large. In addition, the electrons at higher energy penetrate deeper into the bulk and are less sensitive to the surface structure. The high energy end was capped at 350 eV. Different detection window sizes from 100×100 to 41×41 pixels were used; it was found that they all produced very similar I–V data. In the following, we will present the results with a window size of 61×61 pixels. Because of the dead zone on the detector [7], some of the beams were missing in the LEED pattern. Therefore, the detector was rotated to make all the beams detectable. Data were collected at four different detector orientations of 290°, 305°, 320° and 335° respectively. The data were then averaged over equivalent beams and detector orientations to minimize errors due to noise and possible slight deviation from normal incidence. There are totally five inequivalent beams. The cumulative energy range of the averaged data collected for the five beams is 928 eV. As will be shown in the following, the amount of data is sufficient for conducting a complete structural analysis on a 1×1 surface.

3. Theoretical analysis

The calculation was performed using the tensor LEED package [15]. Due to the small interlayer spacings of the MgO(1 1 1) surface, the combined space [16] option in the package was used. Reflection from a composite layer with 12 subplanes was calculated. The top four layers were allowed to relax. The imaginary part of the inner potential was fixed at 5 eV. The optimal surface and bulk vibration amplitudes were found to be 0.20 and 0.15 a.u. respectively. The phase shifts of Mg and O with angular momenta up to $l_{max} = 12$ were obtained by the well-known MUFPOT program, developed by Pendry and co-workers. The non-self-consistent potential used in the program is generated from a charge distribution obtained by overlapping atomic charge densities from neighboring atoms [17]. The charge within the Mg and O muffin-tins were set at +2 and −2 respectively. Hydrogen atoms have very small phase shifts and are not detectable by LEED. Therefore they were not included in the calculation.

As the LEED spectra are mainly due to backscattering of electrons from the atomic core regions, the phase shifts are usually not very sensitive to the detailed charge distribution within the muffin-tins. In most of the surfaces previously studied by LEED [16,18], the MUFPOT phase shifts have consistently produced spectra in good agreement with experiments. However, recent work on TiO_2 [19] has shown that a self-consistent charge distribution is required to fit the experimental LEED data. Therefore we have performed a phase shift calculation using the self-consistent charge distributions of both the surface and bulk atoms of MgO(1 1 1) obtained from a full potential linearized augmented plane wave (FLAPW) calculation [1,20]. It was found that the calculated I–V curves are almost identical to the ones obtained with the non-self-consistent charge distribution from MUFPOT. We have also used the same MUFPOT phase shifts for calculating the I–V spectra of MgO(1 0 0) and compared them with available experimental data [21,22]. They fit quite well with the experiments, which is another indication that the phase shifts are sufficiently accurate for the MgO surfaces. This is different from the case of TiO_2, possibly because the two compounds have very different bulk structures.

4. Results and discussion

The structural search was initialized with the bulk terminated surface. Convergence to within 0.01 Å was achieved only after four iterations. The theoretical I–V curves for the best structure compared with experimental data are shown in Fig. 2. Note that some of the small features in the theoretical curves are smoothed out in the experimental data, possibly due to the presence of disorder and defects on the surface. The LEED spots were also found to be quite broad, which is another indication of surface disorder. The Pendry's R-factor [23] for the best structure is 0.27. There has also been a previous study [1] on the same surface with PhD and DFT. The PhD analysis was based on a limited set of data and was calculated only for eight different possible models predicted by DFT calculations. The data set in the LEED analysis presented here is considerably larger than that used in the PhD study. Therefore it enables us to perform a proper structural search that is not possible with most of the other techniques. In agreement with the PhD and DFT analyses, it was found that the first interlayer spacing is 1.02 Å, close to the interlayer spacing in bulk $Mg(OH)_2$, and much larger than the top layer spacing of 0.86 Å for the oxygen-terminated MgO(1 1 1) surface predicted by DFT calculations [1,3,4]. It is also quite different from the bulk spacing of 1.21 Å for MgO(1 1 1). Though the hydrogen is not directly observable in LEED, this suggests indirectly that the surface is oxygen terminated and covered with hydrogen, forming a surface hydroxide. The second interlayer spacing is found to be expanded by about 3%, which is almost within experimental error of the DFT prediction of a bulk-like spacing. The third interlayer spacing is bulk-like, exactly as found in

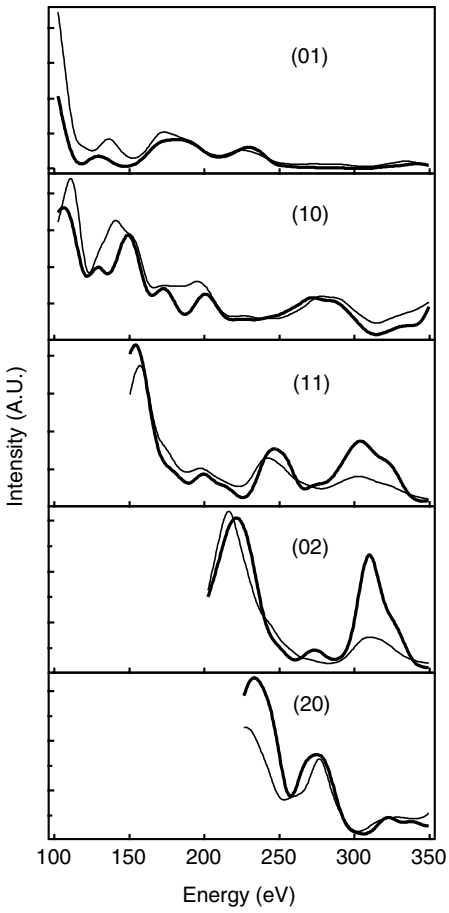

Fig. 2. Comparison of calculated LEED *I–E* curves with the lowest Pendry's *R*-factor (thick solid lines) and corresponding experimental ones (thin solid lines) of diffraction spots (01), (10), (11) (02), and (20) for the MgO(111) (1 × 1) surface.

the DFT calculations. The contour map of the Pendry's *R*-factor as a function of the first and second interlayer spacings with the third interlayer spacing fixed at its optimal value is shown in Fig. 3.

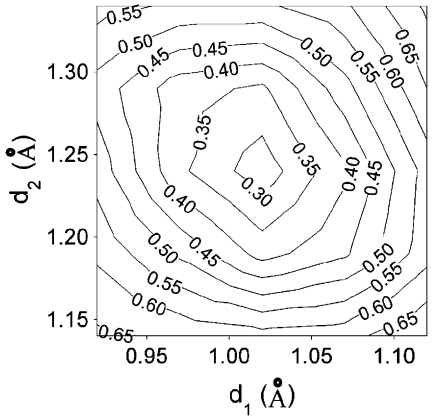

Fig. 3. Contour map of the Pendry's *R*-factor as a function of the first and second interlayer spacings. The third layer spacing (d_3) is fixed at its optimal value of 1.20 Å. The minimum is found for first and second interlayer spacings of $d_1 = 1.02 \pm 0.02$ Å, and $d_2 = 1.24 \pm 0.03$ Å, respectively.

We can estimate the statistical errors by [23]

$$\frac{\Delta R_p}{R_p} = \frac{1}{N^{1/2}} \tag{2}$$

where R_p and ΔR_p are the *R*-factor and its standard deviation and N is the effective number of data points given by

$$N = \frac{\Delta E}{4V_i} \tag{3}$$

where $4V_i$ is the peak width, V_i is the imaginary part of potential. ΔE is the cumulative energy range.

In the present case, $\Delta E = 928$ eV and $V_i = 5$ eV. Therefore $N \approx 46$. Since only the top four layers are allowed to relax, there are only four structural parameters to be determined. It means that the number of effective data points is more than sufficient to solve the 1×1 structure.

By combining Eqs. 2 and 3, we get $\Delta R_p = 0.04$. From the contour map in Fig. 3, the errors in the first two interlayer spacings may be found. We have also conducted the same search with an Mg-terminated surface. The lowest Pendry's *R*-factor in this search was found to be 0.50. Since any deviation of more than $\Delta R_p = 0.04$ from the value of $R_p = 0.27$ found for the hydroxide-terminated model is statistically significant, this effectively rules out an Mg-terminated model. The structural parameters, their errors, and the Pendry's *R*-factors of the different models compared with previous PhD and DFT results are summarized in Table 1. Note that the DFT calculation considered eight different models, some of which have hydrogen below the top layer. Since hydrogen has a very small scattering cross section compared to O and Mg atoms, it has not been considered in our structural analysis. To assess the importance of its effect, a calculation was carried out with the scattering of hydrogen included. The hydrogen atom was put on top of the O atom. It was found that the inclusion of hydrogen leads to the lowering of the *R*-factor from 0.27 to 0.26. The optimal H–O bond length is 0.99 Å, which is quite close to the DFT value of 0.98 Å [1]. It has virtually no effect on the structural parameters with the second interlayer spacing (d_2) increasing slightly by 0.01 Å to 1.25 Å while the other spacings remain unchanged.

We have also considered the possibility of hydrogen desorption induced by incident electrons which leads to

Table 1
Relaxations and Pendry's *R*-factors (R_p) for different surface terminations of MgO(111)-(1 × 1) obtained by LEED compared with results from PhD and DFT calculations [1,4]

	LEED (present work)		PhD and DFT [1]	DFT [1,4]	DFT [1,4]
	Mg terminated	O or OH terminated	OH terminated	O terminated	Mg terminated
d_1 (Å)		1.02 ± 0.02	1.04	0.86	1.25
d_2 (Å)		1.24 ± 0.03	1.21	1.32	1.21
d_3 (Å)		1.20 ± 0.02	1.21	1.14	1.21
R_p	0.50	0.27			

d_1, d_2 and d_3 are the relaxations of the top three interlayer spacings. The bulk spacing is 1.21 Å.

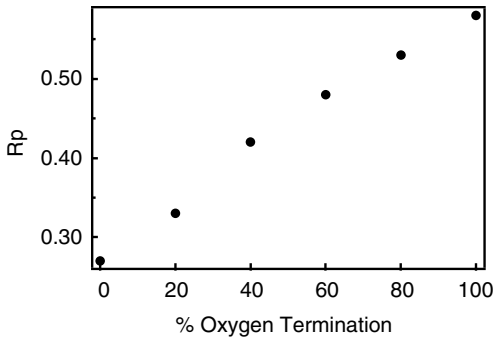

Fig. 4. Pendry's *R*-factor as a function of the percentage of oxygen-terminated domains.

the coexistence of hydroxide-terminated and uncovered (oxygen-terminated) domains. The structures of both domains were fixed (see Table 1) and only the percentage of the oxygen-terminated domain was varied. The Pendry's *R*-factor as a function of the percentage of oxygen-terminated domains is shown in Fig. 4. It shows that the *R*-factor increases with the growth of oxygen-terminated domains, indicating that the electron dose used in the current experiment is too low to cause any damage and the surface is covered with a full monolayer of hydroxide.

5. Conclusions

A structural search has been performed on the 1×1 surface of MgO(1 1 1). Unlike previous PhD and DFT studies that were based on a finite set of models, the analysis presented here is based on an extensive set of *I–V* data which enables us to perform a proper structural search over both the structural and non-structural parameters. In agreement with PhD and DFT analysis, we present here indirect, yet convincing, evidence that the surface is terminated by a hydroxide layer with a O–Mg interlayer distance of 1.02 Å. The second interlayer spacing is found to be expanded by about 3%, although this is within experimental error of the DFT prediction of a bulk-like spacing. Subsequent layers are found to be bulk-like, exactly as predicted by DFT. The current study clearly rules out the possibility of metallization as the stabilization mechanism for the MgO(1 1 1) surface at low temperature, which predicts an O–Mg interlayer distance of 0.86 Å or 1.25 Å, for O and Mg termination, respectively. Due to the beam-charging problem, very few structural studies have been conducted by LEED on insulator surfaces as compared to the large database of structural results with metals and semiconductors. The present study also demonstrates that our new DLD-LEED system is able to produce reliable data for structural analysis, thus opening up the possibility of solving unknown structures of other insulator surfaces by the tried and tested methods of LEED.

Acknowledgements

HCP and DKS (PI) wish to acknowledge support for this work from the US Department of Energy (Grant No. DE-FG02-84ER45076). CJH, XFH and SEC are funded by the grant from the National Science Foundation (NSF-CHE-9984931).

References

[1] V.K. Lazarov, R. Plass, H.-C. Poon, D.K. Saldin, M. Weinert, S.A. Chambers, M. Gajdardziska-Josifovska, Phys. Rev. B 71 (2005) 115434.
[2] K. Refson, R.A. Wogelius, D.G. Fraser, M.C. Payne, M.H. Lee, V. Milman, Phys. Rev. B 52 (1995) 10823.
[3] T. Tsukada, T. Hoshino, Phys. Soc. Jpn. 51 (1982) 2562.
[4] J. Goniakowski, C. Noguera, Phys. Rev. B 60 (1999) 16120.
[5] R. Plass, K. Egan, C. Collazo-Davila, D. Grozea, E. Landree, L.D. Marks, M. Gajdardziska-Josifovska, Phys. Rev. Lett. 81 (1998) 4891.
[6] OCI Microengineering, London, Canada and Reontdek, Frankfurt, Germany.
[7] D. Human, X.F. Hu, C.J. Hirschmugl, J. Ociepa, G. Hall, O. Jagutzki, K. Ullmann-Pfleger, Rev. Sci. Instr. 77 (2006) 023302.
[8] M.M. Albert, N.H. Tolk, Phys. Rev. B 63 (2000) 035308.
[9] T. Fuse, T. Fufino, J.-T. Ryu, M. Katayama, K. Oura, Surf. Sci. 420 (1999) 81.
[10] T.J. Dolan, J. Phys. D: Appl. Phys. 26 (1993) 4.
[11] J.J. Olivero, R.W. Stagat, A.E.S. Green, J. Geophys. Res. 77 (1972) 4797.
[12] A. Jain, J. Phys. B: At. Mol. Opt. Phys. 21 (1988) 905.
[13] D. Ferry, S. Picaud, P.N.M. Hoang, C. Girardet, L. Giordano, B. Demirdjian, J. Suzanne, Surf. Sci. 409 (1998) 101.
[14] J.E. Quinn, Ph.D. thesis, State University of New York at Stony Brook, December 1992.
[15] A. Barbieri, M.A. Van Hove, Symmetrized Automated Tensor LEED package. Available from M.A. Van Hove.
[16] M.A.V. Hove, S.Y. Tong, Surface Crystallography by LEED, Springer, Berlin, 1979.
[17] T. Loucks, Augmented Plane Wave Method, Benjamin, New York, 1967.
[18] J.B. Pendry, Low Energy Electron Diffraction, Academic Press, London, 1974.
[19] R. Lindsay, A. Wander, A. Ernst, B. Montanari, G. Thornton, N.M. Harrison, Phys Rev. Lett. 94 (2005) 246102.
[20] M. Weinert, private communication.
[21] K.O. Legg, M. Prutton, C. Kinniburgh, J. Phys. C 7 (1974) 4236.
[22] T. Urano, T. Kanaji, M. Kaburagi, Surf. Sci. 134 (1983) 109.
[23] J.B. Pendry, J. Phys. C 13 (1980) 937.